Journal of Renewable Materials

Tech Science Press

DOI: 10.32604/jrm.2024.053001

ARTICLE

The Adsorption Properties of TEMPO Oxidized Cellulose against the Mixture of Methylene Blue and Rhemazol Yellow FG

I. Putu Mahendra* **and Kartika Dinita**

Program Studi Kimia, Fakultas Sains, Insitut Teknologi Sumatera, Jalan Terusan Ryacudu, Way Huwi, Jati Agung, Lampung Selatan, 35365, Indonesia

*Corresponding Author: I. Putu Mahendra. Email: i.mahendra@ki.itera.ac.id

Received: 22 April 2024 Accepted: 17 June 2024 Published: 06 September 2024

ABSTRACT

TEMPO/NaOCl/NaBr treatment significantly increased the number of negative charges on the cellulose surface. Two concentrations of NaOCl, 5 and 30 mmol/g of cellulose, were used in this study. The number of carboxyl groups in the two cellulosic samples oxidized using TEMPO/NaOCl/NaBr was 0.5160 and 1.8461 mmol/g of cellulose, respectively. The oxidized cellulose samples treated with 5 and 30 mmol/g NaOCl exhibited higher crystallinity, at 81.15% and 80.14%, respectively, compared to untreated cellulose, which had a crystallinity of 75.95%. The pH effect indicated that the highest adsorption capacity for methylene blue was achieved under alkaline conditions (pH 9), while the highest adsorption capacity for rhemazol yellow FG was achieved under acidic conditions. The kinetic model of TEMPO-oxidized cellulose for methylene blue and rhemazol yellow FG conformed to the pseudo-second-order model. The initial concentration parameter revealed that the isotherm model for the adsorption of methylene blue and rhemazol yellow FG by TEMPO-oxidized cellulose conformed to the Langmuir model. The dye removal efficiencies for methylene blue and rhemazol yellow FG using TEMPO-oxidized cellulose (30 mmol/g) were approximately 80.17% and 59.52%, respectively. These results demonstrate that TEMPO/NaOCl/NaBr-oxidized samples can effectively separate cationic and anionic dye mixtures. Furthermore, the use of TEMPO-oxidized cellulose showed good regeneration capability, maintaining more than 95% of its adsorption capacity after 8 cycles.

KEYWORDS

Cellulose; TEMPO oxidation; cationic and anionic dyes; dye separation

Abbreviations

TEMPO	2,2,6,6-tetramethylpiperidinyloxy
NaOCl	Sodium hypochlorite
NaBr	Sodium bromide

1 Introduction

Water, as a vital source of life, is essential for human beings, fulfilling their fundamental needs. However, with the progression of time and technology, various regions in Indonesia are grappling with the scarcity of clean water due to the rapid growth of industries, particularly the textile industry [1,2].

Rivers in the affected areas have become contaminated due to the discharge of dye waste from textile production processes [3,4].

The textile industry significantly impacts water pollution. Various processes within this industry, primarily the dyeing of fabric materials until the production of ready-to-use textiles, heavily rely on water and chemicals. These chemicals may include heavy metals, dyes, and phenolic compounds, which are often discharged directly into rivers, leading to increased pollution of natural water reservoirs [5–7]. Pollution levels can be monitored through dynamics in parameters such as BOD, COD, TDS, TSS [8–10], and the presence of heavy metals like Cd, Cr, Ni, and Pb [8,11–14].

Numerous methods can be employed to reduce hazardous substances or xenobiotics in water environments, including biological treatment using microorganisms [15], membrane technology [16,17], photocatalysis [18–20], electrochemical [21,22] and adsorption [23–27]. Among these, adsorption processes have gained widespread popularity in waste treatment due to their cost-effectiveness, ease of operation, and capability to remove almost all harmful pollutants [28,29]. Several adsorbents, such as activated carbon, sponge, montmorillonite, zeolite, kaolin, and microbial-based adsorbents, can be used for color waste adsorption [5,30,31]. Another viable alternative for adsorption is bioadsorbents derived from agricultural waste [32–35]. Bioadsorbents offer several advantages, including low cost, easy availability, environmental friendliness, and high adsorption capacity [29,36,37]. Cellulose, a promising material for bioadsorbents in water purification [1,34,38,39], has limitations in color adsorption, as it cannot selectively adsorb specific color groups [28–30]. Colors can be classified into three groups based on their charge in the chemical structure: anionic, cationic, and non-ionic [40]. Therefore, surface modification of cellulose is essential to facilitate interactions with specific color groups. This modification advantageously allows the bound or adsorbed color to be reused in subsequent applications.

Various methods can enhance the ability of cellulose to absorb specific dye groups, including oxidation using periodate, potassium permanganate, and 2,2,6,6-tetramethylpiperidine-1-oxyl (TEMPO) [40–42]. Currently, TEMPO oxidation is widely used for oxidizing cellulose surfaces due to its relatively straightforward process, resulting in the incorporation of numerous carboxylate groups onto the cellulose surfaces. Moreover, TEMPO oxidation can be conducted in water under mild conditions [41–43]. The selective nature of TEMPO oxidation allows for the transformation of hydroxyl groups at the primary C6 position of anhydroglucose units into carboxyl groups on the cellulose surface [44]. Consequently, surface modification of cellulose using TEMPO increases the negative charge content on the cellulose surface, enabling the adsorption of positively charged dye substances. During TEMPO oxidation, several chemicals are normally added as supporting materials, such as NaBr and NaOCl, which are utilized as a co-catalyst and oxidizing agent, respectively. Several studies have evaluated the effect of varying amounts of NaBr and NaOCl on the properties of oxidized cellulose, such as opacity and mechanical properties, which depend on the carboxyl content after TEMPO oxidation. Zhang et al. conducted a study on the effect of NaOCl concentration on TEMPO oxidation, and the resulting fiber was subsequently treated with periodate for further oxidation. The adsorption capacity of the treated fiber was evaluated against chrysoidine and hydrazine [45]. However, the presence of multiple oxidation processes prevents a detailed understanding of the effect of NaOCl concentration on its performance as an adsorbent for chrysoidine and hydrazine due to the subsequent periodate oxidation. Another study by Zhu et al. varied the concentration of NaOCl during TEMPO oxidation and evaluated its performance for humidity sensing [46]. The results confirmed that the NaOCl concentration linearly affected the number of carboxylic groups, and the fiber treated with a high concentration of NaOCl showed the highest performance in humidity sensing.

Based on the theories mentioned above, there was no study that has been performed about the adsorption of the dyes mixture using TEMPO oxidized cellulose. This study focuses on developing oxidized cellulose

using TEMPO/NaBr in the presence of NaOCl at concentrations of 5 and 30 mmol/g of fiber. The goal is to enhance the adsorption of a mixture of methylene blue and rhemazol yellow FG dyes. To support this, various tests were conducted, including Fourier Transform Infrared (FTIR) analysis, Scanning Electron Microscopy (SEM), and X-Ray Diffraction (XRD).

2 Materials and Methods

2.1 Materials

The materials used in this study include sodium hydroxide (NaOH, Glatt Chemical-Indonesia), sodium hypochlorite, 2,2,6,6-tetramethylpiperidine-1-oxyl (TEMPO, Sigma-Singapore), sodium bromide (HiMedia Laboratories-India), deionized water, rhemazol yellow FG (Aman Semesta Enterprise-Malaysia), methylene blue (Sigma-Singapore), hydrochloric acid (BDA Chemical-Indonesia), sodium acetate (Sigma-Singapore), phenolphthalein indicator (Arkitos Chemical-Indonesia), and cellulose (Avicel PH 101, Sigma-Singapore).

2.2 Oxidation of Cellulose Using TEMPO/NaOCl/NaBr

Approximately 0.08 g of TEMPO was dissolved in 500 mL of deionized water, and 5 g of cellulose was added to the TEMPO solution. Sodium bromide (0.05 g) and sodium hypochlorite (NaOCl) at 5 mmol/g were added to the cellulose suspension. The pH of the solution was maintained at 10–11 by adding 5 M sodium hydroxide (NaOH). The cellulose suspension was stirred for 6 h at room temperature, and then the TEMPO-oxidized cellulose was washed with deionized water. The obtained oxidized cellulose was dried at room temperature. The same procedure was repeated with NaOCl at a concentration of 30 mmol/g [47].

2.3 Acid-Base Titration

Approximately 0.1 g of TEMPO-treated cellulose was weighed and acidified using 15 mL of 0.01 M HCl for 1 h. The TEMPO-oxidized cellulose was neutralized by rinsing it with deionized water. The oxidized cellulose was mixed with 50 mL of deionized water and 30 mL of 0.25 M sodium acetate and stirred for 2 h. Then, 30 mL of the mixture was added with one drop of phenolphthalein indicator and titrated using 0.01 M NaOH [48].

2.4 Adsorption Test

Cellulose and TEMPO-oxidized cellulose were subjected to adsorption experiments using several parameters, including pH, contact time, initial concentration, recyclability, and dye separation. The samples were then separated using a centrifuge at 4500 rpm for 10 min. The obtained filtrate was tested using a UV-Vis spectrophotometer. The same procedure was repeated for methylene blue dye and binary mixtures [49,50].

2.5 Fourier Transform Infrared (FTIR) Analysis

FTIR characterization was conducted to analyze the characteristic functional groups of the cellulose samples. Approximately 1 mg of the sample was mixed with 9 mg of KBr, then placed into a press holder and pressed to form a thin pellet. The pellet was inserted into the FTIR compartment (Bruker ALPHA II Compact). FTIR analysis was performed by measuring the transmittance in the wavenumber range of 4000–500 cm^{-1} at a resolution of 4 cm^{-1}.

2.6 Scanning Electron Microscopy (SEM)

The surface morphology of the cellulose and TEMPO-oxidized cellulose powder samples was observed using a Scanning Electron Microscope (SEM TM3000). The samples were coated with gold and then inserted into the specimen chamber. The samples were observed at various magnifications to understand their morphology.

2.7 X-Ray Diffractions (XRD)

XRD analysis was conducted to determine the phase structure and purity of the samples using XRD Rigaku Smartlab. The analysis was performed on cellulose and TEMPO-oxidized cellulose samples. Crystallinity testing was carried out by comparing the distances on the crystal planes and the peak intensities of the diffraction patterns with standard data. The crystallinity index was calculated using the following equation:

Crystallinity index = (crystalline intensity − amorphous intensity)/crystalline intensity × 100%

Data were obtained using an X-ray diffractometer with a Cu Kα radiation source (λ = 1.54060 Å), a scan speed of 1°/0.05 sec, and an initial and final 2θ angle range of 5°–80°.

3 Result and Discussions

The surface modification of cellulose using 2,2,6,6-tetramethylpiperidine-1-oxyl (TEMPO)/NaOCl/NaBr was successfully carried out. TEMPO, a water-soluble compound, acts as a catalyst to oxidize primary hydroxyl groups into aldehyde and carboxylate groups [41–43,47]. Previous studies have documented that increasing the quantity of NaOCl leads to a higher concentration of carboxyl groups on the cellulose surface [47,51]. In this study, two concentrations of NaOCl (5 and 30 mmol/g) were tested for the surface modification of cellulose. The acid-base titration method was used to determine the carboxyl group content in the TEMPO-oxidized cellulose. The amount of carboxyl groups in the TEMPO-oxidized cellulose was found to be 0.5160 mmol/g for the 5 mmol/g NaOCl variation and 1.8461 mmol/g for the 30 mmol/g NaOCl variation. Both cellulose and TEMPO-oxidized cellulose samples with NaOCl concentrations of 5 and 30 mmol/g were analyzed using FTIR to identify the functional groups present. The FTIR spectra are presented in Fig. 1.

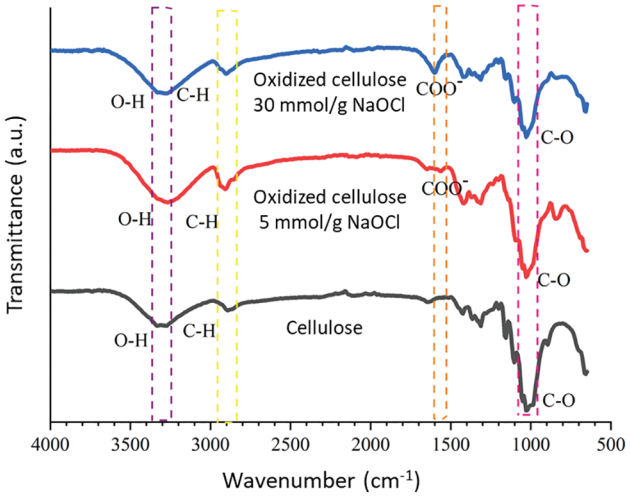

Figure 1: FTIR spectra of cellulose and oxidized cellulose samples

The FTIR spectrum depicted in Fig. 1 illustrates the functional groups present in both the cellulose and TEMPO-oxidized cellulose samples. Despite variations in peak shapes observed among the samples, the resulting spectra exhibit no significant differences. Analysis of the cellulose spectrum reveals the presence of the O-H functional group at 3332 cm^{-1}, with the peak at 2892 cm^{-1} attributed to C-H stretching, and the band at 1028 cm^{-1} indicating C-O stretching. In the spectrum of the TEMPO-oxidized cellulose sample, a distinct peak at 1602 cm^{-1} is observed, corresponding to the carbonyl vibration of carboxylate in its sodium form [5,52–55].

The XRD analysis of cellulose and TEMPO-oxidized cellulose samples treated with NaOCl at concentrations of 5 and 30 mmol/g aimed to identify the phases present in the samples. The XRD results are presented in Fig. 2.

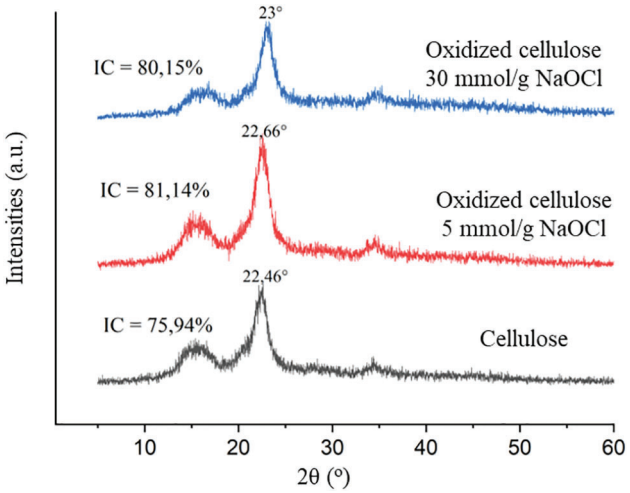

Figure 2: Diffractogram of cellulose and oxidized cellulose

The diffractogram results shown in Fig. 2 confirm that the analyzed cellulose sample belongs to cellulose I, consistent with prior research [56,57]. A shift in the diffraction peaks of the TEMPO-oxidized cellulose sample compared to cellulose is observed. Cellulose and TEMPO-oxidized cellulose at a concentration of 5 mmol/g exhibit crystallinity values of 75.94% and 81.14%, respectively. This increase in crystallinity is attributed to the reduction of amorphous regions on the cellulose surface resulting from its interaction with NaOCl. Oxidation reactions on the amorphous regions eliminate some of the amorphous areas on the cellulose surface. Aldehyde and carboxyl groups are found on both the crystalline and amorphous surfaces of TEMPO-oxidized cellulose, supported by previous studies [42,58,59]. Surface oxidation of cellulose using 30 mmol/g NaOCl results in a slight decrease in crystallinity to 80.15% compared to oxidized cellulose prepared with 5 mmol/g of cellulose. The reduction in cellulose crystallinity is attributed to the increased number of carboxyl groups on the cellulose surface, as indicated by titration results of approximately 1.8461 mmol/g. Several previous studies have reported similar findings regarding the decrease in crystallinity index [54,60–63].

The surface morphology of cellulose and TEMPO-oxidized cellulose samples treated with NaOCl at concentrations of 5 and 30 mmol/g was observed using SEM to determine the structural morphology of the cellulose surface. As shown in Fig. 3, the morphology of cellulose and TEMPO-oxidized cellulose does not differ significantly, and in general, cellulose particles appear to form aggregates. The width dimensions of cellulose and TEMPO-oxidized cellulose were measured using ImageJ 1.8.0. Cellulose exhibited an average width dimension of approximately 8 μm, whereas oxidized cellulose at concentrations of 5 and 30 mmol/g NaOCl displayed decreased average width dimensions of 6 and 4 μm, respectively.

The adsorption experiment focused on TEMPO-oxidized cellulose prepared with 30 mmol/g of NaOCl due to its highest carboxylic content. The presence of carboxylic groups, confirmed through titration, enhances the adsorption capability of TEMPO-oxidized cellulose against cationic dyes, such as methylene blue. Electrostatic interactions play a significant role in the adsorption of methylene blue on the surface of TEMPO-oxidized cellulose (Fig. 4). Fig. 5 illustrates van der Waals interactions occurring during the

adsorption of rhemazol yellow on the surface of TEMPO-oxidized cellulose. Various parameters were utilized in the adsorption experiments, including pH, contact time, and initial concentration.

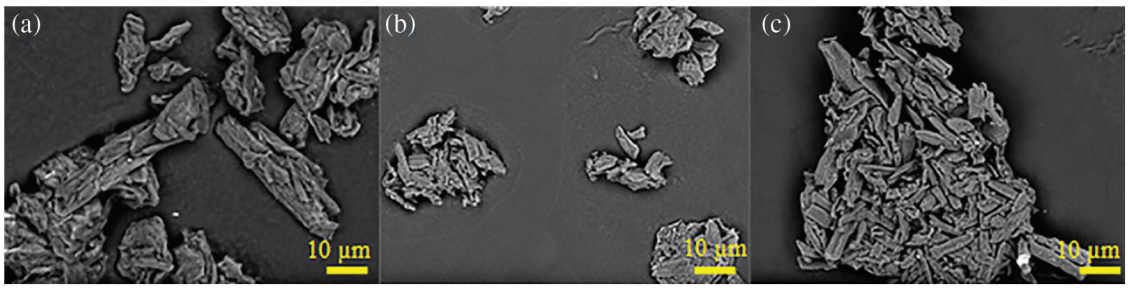

Figure 3: Morphology of (a) cellulose, (b) oxidized cellulose 5 mmol/g NaOCl, and (c) Oxidized cellulose 30 mmol/g NaOCl

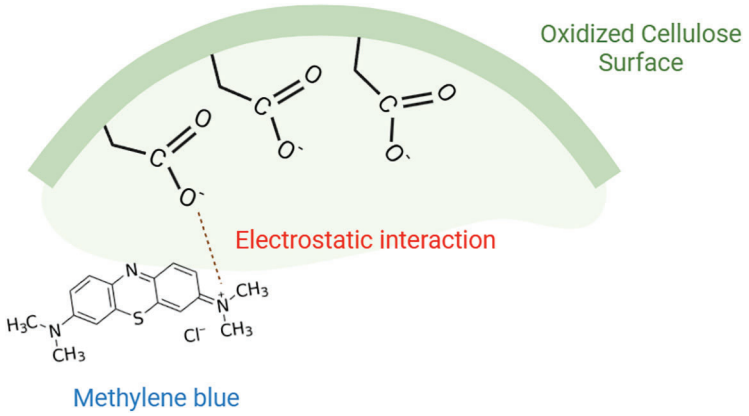

Figure 4: Electrostatic interaction between methylene blue and TEMPO oxidized cellulose

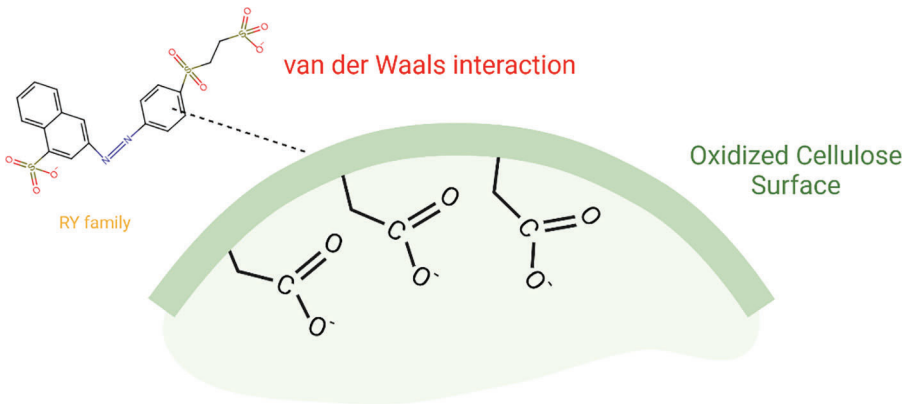

Figure 5: Van der Waals interaction between RY and TEMPO oxidized cellulose

The surface charge of TEMPO-oxidized cellulose was influenced by the pH value of the dye. This study aimed to evaluate the effect of pH on the adsorption performance of TEMPO-oxidized cellulose. The experiments were conducted at pH 5–9 for rhemazol yellow FG and methylene blue. The adsorption capacity of rhemazol yellow FG and methylene blue was determined in separate chambers. Fig. 6

illustrates the adsorption capacity of rhemazol yellow FG and methylene blue. The anionic dye, rhemazol yellow FG, exhibited the highest adsorption capacity in acidic conditions due to the protonation of carboxylic groups. This phenomenon results in the positive charge on the surface of TEMPO-oxidized cellulose. Conversely, under alkaline conditions, the hydrogen from carboxylic groups is deprotonated, resulting in a negative charge on the surface of TEMPO-oxidized cellulose. This explains the highest adsorption capacity of methylene blue (cationic dye) under alkaline conditions.

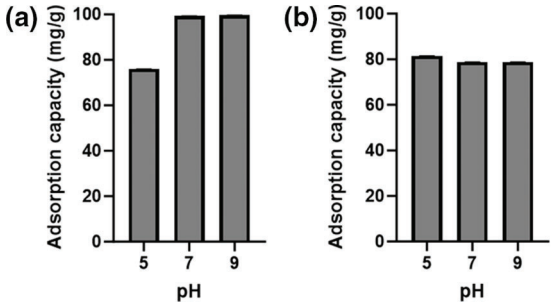

Figure 6: The pH effect on the adsorption capacity of TEMPO oxidized cellulose against (a) methylene blue; (b) rhemazol yellow FG

Contact time during adsorption plays an important role in determining the maximum adsorption capacity at a specific contact time suitable for each dye. In this experiment, the adsorption process was evaluated using pseudo-first and second-order models. Table 1 presents the kinetic parameters of each process. According to Table 1, the adsorption process of methylene blue and rhemazol yellow FG followed the pseudo-second-order model, as concluded from the highest correlation coefficient (R^2) value from each experiment.

Table 1: Kinetic model of dye adsorption by TEMPO oxidized cellulose

Dye	Co (mg/L)	Pseudo first order kinetic model			Pseudo second order kinetic model		
		Qe (mg/g)	k	R^2	Qe (mg/g)	k	R^2
Methylene blue	100	97.35	0.0075	0.965	107.5	1.05×10^{-4}	0.995
	200	181.50	0.0270	0.927	192.05	2.45×10^{-4}	0.965
	400	359.45	0.0090	0.988	403.25	2.90×10^{-5}	0.998
Rhemazol yellow FG	100	92.78	0.0110	0.995	102.75	1.35×10^{-4}	0.997
	200	161.32	0.0125	0.928	174.95	1.03×10^{-4}	0.965
	400	247.05	0.0095	0.920	273.15	5.15×10^{-5}	0.960

The initial concentration is one parameter used to determine the adsorption capacity of the adsorbent. The different values of the initial concentration of the adsorbate would affect the optimum contact time for reaching equilibrium. The adsorption capacities at equilibrium have a linear correlation with the initial concentration. Two isotherm models were used in this study: Langmuir and Freundlich isotherm models.

Fig. 7 and Table 2 present the results of the effect of initial concentrations and the results of Langmuir and Freundlich isotherm models. Data in Table 2 show that the adsorption of methylene blue and rhemazol yellow FG on the matrix of TEMPO oxidized cellulose followed the Langmuir model, as concluded from the highest correlation coefficient (R^2). The Langmuir model suggests that the adsorption process involves monolayer adsorption occurring on the entire surface of TEMPO-oxidized cellulose as the adsorbent

[64–68]. The maximum adsorption capacities (Qm) for methylene blue and rhemazol yellow FG were approximately 601.25 and 320.44 mg/g, respectively. This result confirms that TEMPO oxidized cellulose has better adsorption capacities than adsorbents in previous studies [69–72].

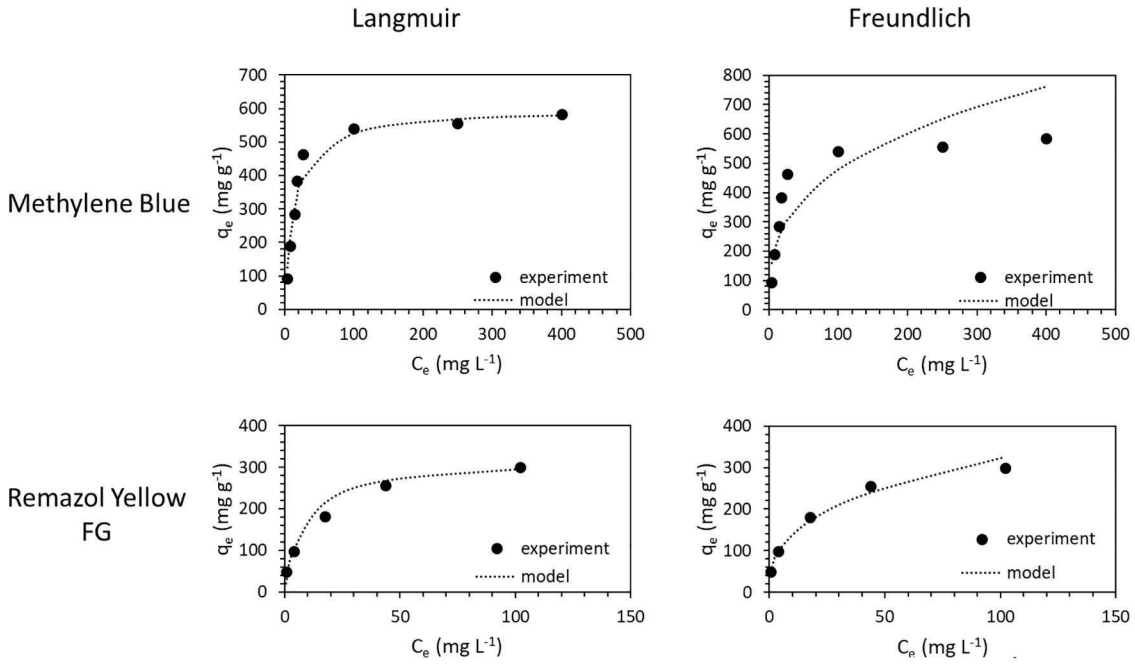

Figure 7: The effect of concentration *vs*. adsorption capacities of TEMPO oxidized cellulose

Table 2: Isotherm model parameters

Isotherm model	Parameters	Methylene blue	Rhemazol yellow FG
Langmuir	Qm	601.25	320.44
	K_L	0.0704	0.1148
	R^2	0.999	0.9948
Freundlich	K_F	102.78	60.77
	n_F	2.9926	2.7532
	R^2	0.7519	0.9933

The utilization of TEMPO-oxidized cellulose as the adsorbent could be employed for several cycles through repeated sorption and desorption processes. Fig. 8 illustrates the different behaviors of TEMPO-oxidized cellulose during the sorption and desorption of methylene blue and rhemazol yellow FG over several cycles. After 8 cycles, the sorption of methylene blue exhibited desirable adsorption capacities, approximately 95%. However, the adsorption capacities of rhemazol yellow FG decreased after several sorption–desorption cycles, reaching approximately 70%. The decrease in the adsorption capacities of rhemazol yellow FG could be caused by the decrease in the availability of binding sites [73–77].

Another experiment was conducted in this study, namely selective adsorption and intelligent separation. The adsorption of a mixed-color solution involves the simultaneous adsorption of methylene blue and

rhemazol yellow FG. The adsorption test was conducted using three samples: cellulose and TEMPO-oxidized cellulose at concentrations of 5 and 30 mmol/g NaOCl. The results of the adsorption experiment for the mixed solution of Rhemazol Yellow FG and methylene blue are depicted in Fig. 9. The percentage adsorption of Rhemazol Yellow FG in the cellulose mixed-color solution was 61.77%. A decrease in the percentage adsorption was observed in the samples of oxidized cellulose at concentrations of 5 and 30 mmol/g NaOCl, with values of 58.32% and 59.52%, respectively.

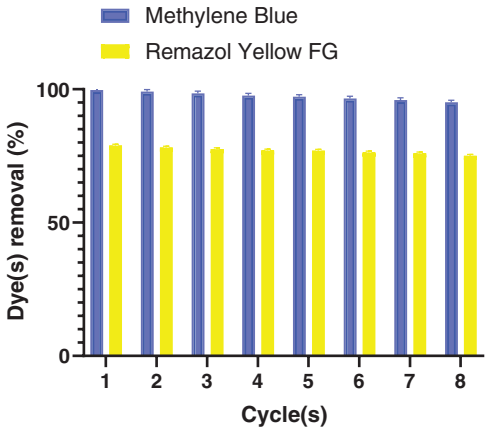

Figure 8: Dye removal performance of TEMPO-oxidized cellulose after 8 cycles

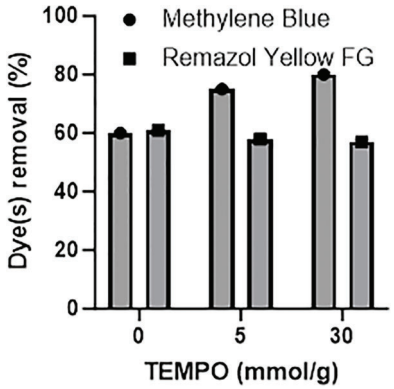

Figure 9: Selective adsorption and intelligent separation of TEMPO-oxidized cellulose

The adsorption test results for methylene blue reveal that TEMPO-oxidized cellulose at 30 mmol/g NaOCl exhibits the highest adsorption at 80.17%. In contrast, the adsorption capacity of cellulose and TEMPO/NaOCl/NaBr-oxidized cellulose at 5 mmol/g was achieved at 60.27% and 75.07%, respectively. The higher content of negatively charged carboxylate groups in the TEMPO-oxidized cellulose samples facilitates interaction with positively charged colorants. This is attributed to the greater abundance of carboxylate groups compared to other samples, allowing for effective adsorption of the positively charged dyes onto the structure of the oxidized cellulose [31,55,78,79].

4 Conclusion

Oxidized cellulose was fabricated using the addition of TEMPO/NaOCl/NaBr, prepared at pH 10–11. The NaOCl concentration has a linear correlation with the carboxylic content of TEMPO-oxidized cellulose. The carboxylic content for NaOCl concentrations of 5 and 30 mmol/g was approximately

0.5160 and 1.8461 mmol/g, respectively. The successful oxidation of cellulose using TEMPO/NaOCl/NaBr was confirmed by the presence of the C = O group. TEMPO-oxidized cellulose has a higher crystallization index than cellulose. The maximum adsorption capacities of TEMPO-oxidized cellulose (30 mmol/g) against methylene blue and rhemazol yellow FG were approximately 601.25 and 320.44 mg/g, respectively. The recyclability of TEMPO-oxidized cellulose shows good performance for up to 8 cycles, with sorption capacities of methylene blue reaching up to 95%, although a decrease was observed for rhemazol yellow FG. Due to the presence of carboxylic groups on the surface of TEMPO-oxidized cellulose, the prepared adsorbent could separate the anionic and cationic groups. The degree of removal of anionic and cationic dyes depends on the amount of carboxylic content.

Declaration of Generative AI and AI-Assisted Technologies in the Writing Process: During the preparation of this work, the authors used Grammarly and OpenAI (GPT-3.5) in order to improve the language and readability. After using this tool/service, the authors reviewed and edited the content as needed and takes full responsibility for the content of the publication.

Acknowledgement: This study was supported by Institut Teknologi Sumatera through GBU 45 Research Grant.

Funding Statement: This study was supported by Institut Teknologi Sumatera through GBU 45 Research Grant with a Contract Number B/763c/IT9.C1/PT.01.03/2022.

Author Contributions: The authors confirm contribution to the paper as follows: study conception and design: I. Putu Mahendra, Kartika Dinita; data collection: Kartika Dinita; analysis and interpretation of results: I. Putu Mahendra, Kartika Dinita; draft manuscript preparation: I. Putu Mahendra, Kartika Dinita. All authors reviewed the results and approved the final version of the manuscript.

Availability of Data and Materials: The authors declare that the data supporting the findings of this study are available within the paper. Should any raw data files be needed in another format, they are available from the corresponding author upon reasonable request.

Conflicts of Interest: The authors declare that they have no conflicts of interest to report regarding the present study.

References

1. Putro JN, Kurniawan A, Ismadji S, Ju YH. Nanocellulose based biosorbents for wastewater treatment: study of isotherm, kinetic, thermodynamic and reusability. Environ Nanotechnol Monit Manag. 2017;8:134–49.
2. Darmawan A, Fuad K, Azmiyawati C. Synthesis of chromium pillared clay for adsorption of methylene blue. IOP Conf Ser Mater Sci Eng. 2019;509:012003.
3. Aryanti N, Nafiunisa A, Kusworo TD, Wardhani DH. Separation of reactive dyes using natural surfactant and micellar-enhanced ultrafiltration membrane. J Memb Sci Res. 2021;7:20–8.
4. Aryanti N, Nafiunisa A, Irmalasari LN, Nisa IMK, Wardhani DH. Treatment of batik wastewater using plant derived surfactant-enhanced ultrafiltration membrane. IOP Conf Ser Mater Sci Eng. 2019;620:012015.
5. Batmaz R, Mohammed N, Zaman M, Minhas G, Berry RM, Tam KC. Cellulose nanocrystals as promising adsorbents for the removal of cationic dyes. Cellulose. 2014;21:1655–65.
6. Azizah DA, Kusworo TD, Kumoro AC. Developing UV-light driven photocatalytic PSf/Ni-doped ZnO/PDA membrane with superior antifouling, self-cleaning, and self-protecting performances for handmade batik wastewater treatment. Mater Today Sustain. 2024;26:100721.
7. Kusworo TD, Azizah DA, Kumoro AC, Kurniawan TA, Dzarfan Othman MH. Fabrication, characterization, and application of PSf/Ni@ZnO amalgamated membrane for photocatalytic degradation of dyeing wastewater from batik industry. Mater Today Chem. 2023;30:101493.

8. Maslukah L, Wirasatriya A, Yusuf M, Sari RS, Salma U, Zainuri M. Phosphorous fractionation distribution in surface sediments of the Jobokuto Bay. Molekul. 2021;16(2):100. doi:10.20884/1.jm.2021.16.2.572.
9. Syafrudin S, Sarminingsih A, Juliani H, Budihardjo MA, Puspita AS, Auliya Arlin Mirhan S. Water quality monitoring system for temperature, pH, turbidity, DO, BOD, and COD parameters based on internet of things in garang watershed. Ecol Eng Environ Technol. 2024;25(2):1–16. doi:10.12912/27197050/174412.
10. Larasati DA, Alkian I, Arifan F, Sari SR. Batik home industry wastewater treatment using UVC/Ozon oxidation method: case study in Cibelok village, Pemalang, Indonesia. IOP Conf Ser Earth Environ Sci. 2020;448:012055.
11. Wenten IG, Khoiruddin K, Wardani AK, Widiasa IN. Synthetic polymer-based membranes for heavy metal removal. In: Synthetic polymeric membranes for advanced water treatment, gas separation, and energy sustainability. Elsevier; 2020. p. 71–101.
12. Arief Budihardjo M, Purwono, Selfi Nugraheni A. Analysis of groundwater quality surrounding municipal solid waste landfill: banyuurip landfill, Magelang, Indonesia. MATEC Web Conf. 2018;159:01031.
13. Ariyanti D, Lesdantina D, Purbasari A, Astuti Y. Synthesis of graphene-like material derived from biomass from agricultural waste and its application in Cu (II) removal. Korean J Chem Eng. 2023;40(4):964–74. doi:10.1007/s11814-023-1380-8.
14. Wijaya A, Semedi B, Lusiana R, Armid A, Muntholib M. Metal contents and Pb Isotopes in the surface seawater of the gulf of Prigi, Indonesia: detection of anthropogenic and natural sources. J Braz Chem Soc. 2018.
15. Piaskowski K, Świderska-Dąbrowska R, Zarzycki PK. Dye removal from water and wastewater using various physical, chemical, and biological processes. J AOAC Int. 2018;101(5):1371–84. doi:10.5740/jaoacint.18-0051.
16. Aryanti N, Nafiunisa A, Adina AR, Kusworo TD. Synthesis, characterization and anti-fouling properties of poly [vinylidene fluoride]-incorporated SiO_2, TiO_2, ZrO_2 nanoparticle-LiCl pore former ultrafiltration membranes. Case Stud Chem Environ Eng. 2024;9(11):100664. doi:10.1016/j.cscee.2024.100664.
17. Sabri NSM, Hasbullah H, Jye LW, Sadikin AN, Ibrahim N, Rahman SA, et al. Permeable and antifouling PSf-Cys-CuO ultrafiltration membrane for separation of biological macromolecules proteins. Environ Qual Manag. 2024;33(3):103–12. doi:10.1002/tqem.21995.
18. Utomo DP, Kusworo TD, Kumoro AC, Othman MHD. Developing a versatile and resilient PVDF/CeO_2@GO-COOH photocatalytic membrane for efficient treatment of antibiotic-contaminated wastewater. J Water Process Eng. 2023;56:104353. doi:10.1016/j.jwpe.2023.104353.
19. Nurhasanah I, Rohmaniah S, Astuti Y, Kinasih DA. Efficient degradation of pharmaceutical drugs using cerium-doped zinc oxide nanophotocatalysts synthesized via the sono-precipitation route. Nanotechnol Environ Eng. 2023;8(4):899–909. doi:10.1007/s41204-023-00340-x.
20. Widiyandari H, Prilita O, Al Ja'farawy MS, Nurosyid F, Arutanti O, Astuti Y, et al. Nitrogen-doped carbon quantum dots supported zinc oxide (ZnO/N-CQD) nanoflower photocatalyst for methylene blue photodegradation. Results Eng. 2023;17(5):100814. doi:10.1016/j.rineng.2022.100814.
21. Mukimin A, Vistanty H, Harihastuti N, Setianingsih NI, Djayanti S, Nilawati, et al. Hybrid Fenton-electrochemical reactor and system as post-treatment of textile wastewater. J Water Process Eng. 2024;59(2):105028. doi:10.1016/j.jwpe.2024.105028.
22. Sajjadizadeh HS, Goharshadi EK, Ahmadzadeh H. Photoelectrochemical water splitting by engineered multilayer TiO_2/GQDs photoanode with cascade charge transfer structure. Int J Hydrogen Energy. 2020;45(1):123–34. doi:10.1016/j.ijhydene.2019.10.161.
23. Yang X, Liu H, Han F, Jiang S, Liu L, Xia Z. Fabrication of cellulose nanocrystal from Carex meyeriana Kunth and its application in the adsorption of methylene blue. Carbohydr Polym. 2017;175(2):464–72. doi:10.1016/j.carbpol.2017.08.007.
24. Ardhianto R, Anggrainy AD, Samudro G, Triyawan A, Bagastyo AY. A study of continuous-flow electrocoagulation process to minimize chemicals dosing in the full-scale treatment of plastic plating industry wastewater. J Water Process Eng. 2024;60:105217. doi:10.1016/j.jwpe.2024.105217.
25. Kusworo TD, Kumoro AC, Puspa MB, Citradhitya P, Utomo DP. Removal of ciprofloxacin-humic acid pollutant residue in wastewater through a hybrid treatment system consisting of pre-treatment with ozonation-AC/TiO_2/

CeO_2 adsorption and degradation using PVDF/Ni-CeO_2@SiO_2 photocatalytic membrane. J Environ Chem Eng. 2024;12(2):112216. doi:10.1016/j.jece.2024.112216.

26. Roslan NN, Lau HLH, Suhaimi NAA, Shahri NNM, Verinda SB, Nur M, et al. Recent advances in advanced oxidation processes for degrading pharmaceuticals in wastewater—a review. Catalysts. 2024;14(3):189. doi:10.3390/catal14030189.
27. Wibowo YG, Taher T, Khairurrijal K, Ramadan BS, Safitri H, Sudibyo S, et al. Recent advances in the adsorptive removal of heavy metals from acid mine drainage by conventional and novel materials: a review. Bioresour Technol Rep. 2024;25:101797.
28. Ali I. New generation adsorbents for water treatment. Chem Rev. 2012;112:5073–91.
29. Lin F, You Y, Yang X, Jiang X, Lu Q, Wang T, et al. Microwave-assisted facile synthesis of TEMPO-oxidized cellulose beads with high adsorption capacity for organic dyes. Cellulose. 2017;24:5025–40.
30. Li D, Tian X, Wang Z, Guan Z, Li X, Qiao H, et al. Multifunctional adsorbent based on metal-organic framework modified bacterial cellulose/chitosan composite aerogel for high efficient removal of heavy metal ion and organic pollutant. Chem Eng J. 2020;383:123127.
31. Benhalima T, Chicha W, Ferfera-Harrar H. Sponge-like biodegradable polypyrrole-modified biopolymers for selective adsorption of basic red 46 and crystal violet dyes from single and binary component systems. Int J Biol Macromol. 2023;253:127532.
32. Budihardjo MA, Wibowo YG, Ramadan BS, Serunting MA, Yohana E, Syafrudin. Mercury removal using modified activated carbon of peat soil and coal in simulated landfill leachate. Environ Technol Innov. 2021;24:102022.
33. Sari AA, Akhmad RIS, Asmara AA, Arutanti O, Hadibarata T, Andreas, et al. Characterization and mechanisms of a new carbonaceous adsorbent based on black liquor loaded with iron oxide for removal of tripolyphosphate Ions. Water Air Soil Pollut. 2020;231:449.
34. Sumiyati S, Huboyo HS, Ramadan BS. Potential use of banana plant (*Musa spp*.) as bio-sorbent materials for controlling gaseous pollutants. E3S Web Conf. 2019;125:03015.
35. Supriyantini E, Soenardjo N, Santosa GW, Ridlo A, Sedjati S, Ambariyanto A. Effectiveness and efficiency of the red seaweed Gracilaria verrucosa as biofilter in Pb absorption in seawater. AACL Bioflux. 2018;11:877–83.
36. Wibowo YG, Sudibyo, Naswir M, Ramadan BS. Performance of a novel biochar-clamshell composite for real acid mine drainage treatment. Bioresour Technol Rep. 2022;17:100993.
37. Purbasari A, Ariyanti D, Sumardiono S, Khairunnisa K, Sidharta T. Adsorption kinetics and isotherms of Cu(II) and Fe(II) Ions from aqueous solutions by fly ash-based geopolymer. Chem Chem Technol. 2022;16:169–76.
38. Wahyudi RS, Huboyo HS, Zaman B. Removal of hydrogen sulfide gas pollutants with various wet banana leaf types. Water Air Soil Pollut. 2023;234:288.
39. Kusworo TD, Soetrisnanto D, Utomo DP. Development of nano-hybrid cellulose acetate/TiO_2 membrane for eugenol purification from crude clove leaf oil. MATEC Web Conf. 2018;156:08013.
40. Vega-Negron AL, Alamo-Nole L, Perales-Perez O, Gonzalez-Mederos AM, Jusino-Olivencia C, Roman-Velazquez FR. Simultaneous adsorption of cationic and anionic dyes by chitosan/cellulose beads for wastewaters treatment. Int J Environ Res. 2018;12:59–65.
41. Saito T, Isogai A. Introduction of aldehyde groups on surfaces of native cellulose fibers by TEMPO-mediated oxidation. Colloids Surf A Physicochem Eng Asp. 2006;289:219–25.
42. Saito T, Isogai A. TEMPO-mediated oxidation of native cellulose. The effect of oxidation conditions on chemical and crystal structures of the water-insoluble fractions. Biomacromolecules. 2004;5:1983–9. doi:10.1021/bm0497769.
43. Isogai A, Saito T, Fukuzumi H. TEMPO-oxidized cellulose nanofibers. Nanoscale. 2011;3:71–85.
44. Milanovic J, Kostic M, Skundric P. Structure and properties of tempo-oxidized cotton fibers. Chem Ind Chem Eng Q. 2012;18:473–81.
45. Zhang Z, Liu L, Ma H, Venkateswaran S, Hsiao BS. Periodate and TEMPO sequential oxidations of cellulose fabrics: exploration of a multiple and synergistic adsorption mechanism. Sep Purif Technol. 2024;330:125388.

46. Zhu J, Zhu P, Zhu Y, Ye Y, Sun X, Zhang Y, et al. Surface charge manipulation for improved humidity sensing of TEMPO-oxidized cellulose nanofibrils. Carbohydr Polym. 2024;335:122059.
47. Mahendra IP, Wirjosentono B, Ismail H, Mendez JA. Thermal and morphology properties of cellulose nanofiber from TEMPO-oxidized lower part of empty fruit bunches (LEFB). Open Chem. 2019;17(1):526–36. doi:10.1515/chem-2019-0063.
48. Kumar V, Yang T. HNO_3/H_3PO_4-$NANO_2$ mediated oxidation of cellulose—preparation and characterization of bioabsorbable oxidized celluloses in high yields and with different levels of oxidation. Carbohydr Polym. 2002;48(4):403–12. doi:10.1016/S0144-8617(01)00290-9.
49. Tolkou AK, Tsoutsa EK, Katsoyiannis IA, Kyzas GZ. Simultaneous removal of anionic and cationic dyes on quaternary mixtures by adsorption onto banana, orange and pomegranate peels. Colloids Surf A Physicochem Eng Asp. 2024;685:133176. doi:10.1016/j.colsurfa.2024.133176.
50. Mehdi SU, Balamirtham H, Aravamudan K. Optimal adsorption of a binary dye mixture of basic yellow 2 and rhodamine B using mixture-process variable design, ridge analysis and multi-objective optimization. Environ Adv. 2024;15(2):100490. doi:10.1016/j.envadv.2024.100490.
51. Okita Y, Saito T, Isogai A. Entire surface oxidation of various cellulose microfibrils by TEMPO-mediated oxidation. Biomacromolecules. 2010;11(6):1696–700. doi:10.1021/bm100214b.
52. Abou-Zeid RE, Salama A, Al-Ahmed ZA, Awwad NS, Youssef MA. Carboxylated cellulose nanofibers as a novel efficient adsorbent for water purification. Cellulose Chem Technol. 2020;54:237–45.
53. Zhang K, Sun P, Liu H, Shang S, Song J, Wang D. Extraction and comparison of carboxylated cellulose nanocrystals from bleached sugarcane bagasse pulp using two different oxidation methods. Carbohydr Polym. 2016;138:237–43.
54. Yang H, Alam MDN, Van de Ven TGM. Highly charged nanocrystalline cellulose and dicarboxylated cellulose from periodate and chlorite oxidized cellulose fibers. Cellulose. 2013;20:1865–75.
55. Benhalima T, Ferfera-Harrar H, Saha N, Saha P. Fe_3O_4 imbuing carboxymethyl cellulose/dextran sulfate nanocomposite hydrogel beads: an effective adsorbent for methylene blue dye pollutant. J Macromolecular Sci, A. 2023;60:442–61.
56. Mittal A, Katahira R, Himmel ME, Johnson DK. Effects of alkaline or liquid-ammonia treatment on crystalline cellulose: changes in crystalline structure and effects on enzymatic digestibility. Biotechnol Biofuels. 2011;4:41.
57. Nelson ML, O'Connor RT. Relation of certain infrared bands to cellulose crystallinity and crystal lattice type. Part II. A new infrared ratio for estimation of crystallinity in celluloses I and II. J Appl Polym Sci. 1964;8(3):1325–41. doi:10.1002/app.1964.070080323.
58. Baron RI, Coseri S. Preparation of water-soluble cellulose derivatives using TEMPO radical-mediated oxidation at extended reaction time. React Funct Polym. 2020;157:104768. doi:10.1016/j.reactfunctpolym.2020.104768.
59. Huang C, Ji H, Yang Y, Guo B, Luo L, Meng Z, et al. TEMPO-oxidized bacterial cellulose nanofiber membranes as high-performance separators for lithium-Ion batteries. Carbohydr Polym. 2020;230(38):115570. doi:10.1016/j.carbpol.2019.115570.
60. Calderón-Vergara LA, Ovalle-Serrano SA, Blanco-Tirado C, Combariza MY. Influence of post-oxidation reactions on the physicochemical properties of TEMPO-oxidized cellulose nanofibers before and after amidation. Cellulose. 2020;27(3):1273–88. doi:10.1007/s10570-019-02849-4.
61. Kuramae R, Saito T, Isogai A. TEMPO-oxidized cellulose nanofibrils prepared from various plant holocelluloses. React Funct Polym. 2014;85:126–33. doi:10.1016/j.reactfunctpolym.2014.06.011.
62. Saito T, Okita Y, Nge TT, Sugiyama J, Isogai A. TEMPO-mediated oxidation of native cellulose: microscopic analysis of fibrous fractions in the oxidized products. Carbohydr Polym. 2006;65:435–40.
63. Tanaka R, Saito T, Isogai A. Cellulose nanofibrils prepared from softwood cellulose by TEMPO/NaClO/$NaClO_2$ systems in water at pH 4.8 or 6.8. Int J Biol Macromol. 2012;51:228–34.
64. Shahrin EWES, Narudin NAH, Shahri NNM, Verinda SB, Nur M, Hobley J, et al. Adsorption behavior and dynamic interactions of anionic acid blue 25 on agricultural waste. Molecules. 2022;27:1718.
65. Utami UBL, Cahyono B, Susanto H. Isotherms and capacity adsorption of Fe(III) onto duck feather modification using CH_3OH and HCl solution. Rasayan J Chem. 2020;13:2106–13.

66. Santosa SJ, Siswanta D, Kurniawan A, Rahmanto WH. Hybrid of chitin and humic acid as high performance sorbent for Ni(II). Surf Sci. 2007;601:5155–61.
67. Azmiyawati C, Nuryono N, Narsito N. Adsorption of Mg(II) and Ca(II) on disulfonato-silica hybrid. Indones J Chem. 2012;12:223–8.
68. Purbasari A, Ariyanti D, Sumardiono S, Shofa M, Manullang R. Comparison of alkali modified fly ash and alkali activated fly ash as Zn(II) ions adsorbent from aqueous solution. Sci Sintering. 2022;54:49–58.
69. Yang L, Bao L, Dong T, Xie H, Wang X, Wang H, et al. Adsorption properties of cellulose/guar gum/biochar composite hydrogel for Cu^{2+}, Co^{2+} and methylene blue. Int J Biol Macromol. 2023;242:125021.
70. Xiong J, Zhang D, Lin H, Chen Y. Amphiprotic cellulose mediated graphene oxide magnetic aerogels for water remediation. Chem Eng J. 2020;400:125890.
71. Sajab MS, Chia CH, Chan CH, Zakaria S, Kaco H, Chook SW, et al. Bifunctional graphene oxide-cellulose nanofibril aerogel loaded with Fe(III) for the removal of cationic dye via simultaneous adsorption and Fenton oxidation. RSC Adv. 2016;6:19819–25.
72. Eltaweil AS, Elgarhy GS, El-Subruiti GM, Omer AM. Carboxymethyl cellulose/carboxylated graphene oxide composite microbeads for efficient adsorption of cationic methylene blue dye. Int J Biol Macromol. 2020;154:307–18.
73. Azmiyawati C, Virkyanov T. Synthesis of thiazole silica hybrid from waste glass for adsorption of cadmium(II). IOP Conf Ser Mater Sci Eng. 2016;107:012009.
74. Arnelli, Aditama WP, Fikriani Z, Astuti Y. Adsorption kinetics of surfactants on activated carbon. IOP Conf Ser Mater Sci Eng. 2018;349:012001.
75. Purbasari A, Ariyanti D, Fitriani E. Adsorption of methyl orange dye by modified fly ash-based geopolymer—characterization, performance, kinetics and isotherm studies. J Ecol Eng. 2023;24:90–8.
76. Shahrin EWES, Narudin NAH, Shahri NNM, Nur M, Lim JW, Bilad MR, et al. A comparative study of adsorption behavior of rifampicin, streptomycin, and ibuprofen contaminants from aqueous solutions onto chitosan: dynamic interactions, kinetics, diffusions, and mechanisms. Emerg Contam. 2023;9:100199.
77. Ismanto A, Sukmono Y, Hadibarata T, Yeow PK, Indrayanti E, Ismunarti DH, et al. Removal of Remazol brilliant blue r and Remazol brilliant violet 5r dyes from aqueous solution by adsorption using coffee residue. Environ Qual Manag. 2023;33(4):47–57.
78. Pottathara YB, Narwade VN, Bogle KA, Kokol V. TEMPO-oxidized cellulose nanofibrils-graphene oxide composite films with improved dye adsorption properties. Polym Bull. 2020;77:6175–89.
79. Hussain A, Li J, Wang J, Xue F, Chen Y, Bin Aftab T, et al. Hybrid monolith of graphene/TEMPO-oxidized cellulose nanofiber as mechanically robust, highly functional, and recyclable adsorbent of methylene blue dye. J Nanomater. 2018;2018(3):1–12. doi:10.1155/2018/5963982.